journal

J. Am. Ceram. Soc., 86 [11] 1933–39 (2003)

Surface Energy Anisotropy of $SrTiO_3$ at 1400°C in Air

Tomoko Sano,† David M. Saylor,‡ and Gregory S. Rohrer*,†

Department of Materials Science and Engineering, Carnegie Mellon University, Pittsburgh, Pennsylvania 15213-3890

National Institute of Standards and Technology, Gaithersburg, Maryland 20899

Geometric and crystallographic measurements of grain-boundary thermal grooves and surface faceting behavior as a function of orientation have been used to determine the surface energy anisotropy of $SrTiO_3$ at 1400°C in air. Under these conditions, thermal grooves are formed by surface diffusion. The surface energy anisotropy was determined using the capillarity vector reconstruction method under the assumption that Herring's local equilibrium condition holds at the groove root. The results indicate that the (100) surface has the minimum energy. For surfaces inclined between 0° and 30° from (100), the energy increases with the inclination angle. Orientations inclined by more than 30° from (100) are all about 10% higher in energy and, within experimental uncertainty, energetically equivalent. A procedure for estimating the uncertainties in the reconstructed energies is also introduced. Taken together, the orientation dependence of the surface-facet formation and the measured energy anisotropy lead to the conclusion that the equilibrium crystal shape is dominated by {100}, but also includes {110} and {111} facets. Complex planes within about 15° of {100} and 5° of {110} are also part of the equilibrium shape.

I. Introduction

DURING the initial stages of pressureless sintering, the primary driving force for shape changes of the small particles is surface energy reduction. These morphologic changes reduce the driving force for sintering without necessarily increasing the density of the product. The magnitude of this driving force reduction is difficult to quantify since little is known about surface energy anisotropies of ceramics. Most of what we know is derived from studies of pores. The state-of-the-art is represented by recently reported observations of small pores in alumina at a range of temperatures and in the presence of certain impurities.[1–3] An alternative method for determining the surface energy anisotropy is based on the analysis of the shapes of thermal grooves formed at circumferential grain boundaries.[4,5] In this method, a model for the surface energy as a function of surface normal, $\gamma(\mathbf{n})$, is determined by assuming that the thermal groove is in local thermodynamic equilibrium, as described by Herring.[6] The exact shape of $\gamma(\mathbf{n})$ that results from this analysis depends on the method used to fit the observations to the equilibrium condition. A comparison of two different methods of interpreting the data illustrated that the capillarity vector reconstruction method[5] reproduces the true anisotropy more faithfully than an earlier series fitting method.[4]

The capillarity vector reconstruction method is a numerical procedure for finding a set of interface energies that best satisfy the Herring condition at a set of observed triple junctions. For numerical simplicity, the Herring condition is expressed using the capillarity vector formalism developed by Cahn and Hoffman:[7,8]

$$(\boldsymbol{\xi}^1 + \boldsymbol{\xi}^2 + \boldsymbol{\xi}^3) \times \mathbf{l} = 0 \quad (1)$$

In Eq. (1), $\boldsymbol{\xi}^1$, $\boldsymbol{\xi}^2$, and $\boldsymbol{\xi}^3$ are the capillarity vectors associated with the two free surfaces and the grain boundary, respectively, and $\mathbf{l}$ is the unit vector pointing along the line where the three interfaces meet. For every observed groove root, there is a separate equilibrium equation with the form of Eq. (1), for which we have measured the direction of $\mathbf{l}$ and the directions of the two perpendicular components of each $\boldsymbol{\xi}$ vector. The only unknowns are the magnitudes of the vectors. It is important that the number of unknown parameters is smaller than the number of observations. Therefore, the domain of distinguishable surface normals is discretized, and the number of distinct grain boundaries is limited by making many measurements at a small set of circumferential thermal grooves. To further simplify the problem, we make the approximation that the energy of each grain boundary is independent of the interface plane. The errors arising from this approximation are expected to change signs around the groove circumference and, therefore, partially cancel as data from a large number of grooves is averaged. Using this approximation, each circumferential groove adds only a single unknown parameter to the set of equilibrium equations. Therefore, after a sufficient number of observations, an iterative procedure, originally described by Morawiec,[9] can be used to find the set of capillarity vectors that most nearly satisfies this system of linear equations.

In the current paper, we present an analysis of the surface energy anisotropy of $SrTiO_3$. This compound was selected primarily because it is a prototypical example of a wide variety of cubic perovskite materials. However, its surface properties are of interest for potential applications as a substrate for heteroepitaxial films[10] and as a new gate dielectric for field-effect transistors.[11]

II. Experimental Procedure

The polycrystalline sample studied here was fabricated from 99% pure $SrTiO_3$ powder (Aldrich Chemical Co., Inc., Milwaukee, WI).[12] The disk-shaped specimen was consolidated by uniaxial compaction. Before sintering, the sample was degassed by heating under vacuum (16 kPa) at 800°C for 25 h. A flow of reconditioned air was then established, and the temperature was increased to 1350°C at 3°C/min and held for 10 h. To enlarge the grain size, the sample was heated for an additional 20 h at 1650°C in static air. Orientation imaging microscopy was used to examine the microstructure, and on the basis of measuring areas of constant orientation, the final grain size was found to be ~90 μm. The sample was then lapped flat with a 3-μm alumina slurry and polished with a 0.02-μm colloidal silica slurry. The final surface was flat to within ±0.2 μm over the entire sample surface.

Thermal grooves were observed at a range of temperatures between 1300° and 1400°C. The characteristic shape of the grooves formed in the lower part of this temperature range

J. E. Blendell—contributing editor

Manuscript No. 10084. Received March 27, 2003; approved May 29, 2003.

This work was supported primarily by NASA under Grant No. 8-1674, and partial support was from the MRSEC program of the National Science Foundation under Award No. DMR-0079996.

*Member, American Ceramic Society.

†Carnegie Mellon University.

‡National Institute of Standards and Technology.

suggests that the dominant atomic removal mechanism was evaporation, while the shapes of grooves formed at the highest temperature were characteristic of those formed by surface diffusion.[13] For the experiments described here, all the thermal grooves were formed at 1400°C. To form the grooves, the sample temperature was ramped from ambient to 1100°C at 10°C/min, and then from 1100° to 1400°C at 30°C/min; the sample was then held at this temperature for 6–60 min before cooling. The grooves formed in 6 min were ~2 μm wide and suitable for our measurements. Longer times were used to examine the kinetics of groove formation.

After forming thermal grooves, optical micrographs of included grains with circumferential boundaries were recorded. A thin layer (4.65 ± 0.3 μm) of the sample was then removed by polishing, the grooving process was repeated, and the same grains were located and examined in detail. To determine $\gamma(\mathbf{n})$, it is necessary to characterize the normal and tangent directions to all three interfaces at the groove root, in the crystal reference frame. Crystal orientation measurements were made using electron backscattered diffraction patterns (EBSPs) in the scanning electron microscope (SEM), and the groove and surface geometries were measured using atomic force microscopy (AFM). The inclination of the grain-boundary plane was determined by comparing the apparent position of the boundary on the two parallel-section planes. The procedures used for these measurements have already been described in detail.[4]

It should be noted that because thermal grooves are concave and have a constantly changing slope, measuring the exact profile is difficult.[14] Measurements of the slope at the groove root directly from AFM profiles have unavoidable errors. A previous analysis of the problem illustrated that these errors can be largely avoided by assuming that the groove has a known quasi-static profile and then finding the slope at the groove root based on measurements of the depth and width of sufficiently large grooves.[15] There is an inherent approximation in this procedure, since the quasi-static profile was determined under the assumption that the surface energy is isotropic. This creates an error in the determination of the surface orientation at the groove root. However, since the majority of the observed grooves have profiles that approximate the expected quasi-static shape, and past results obtained by this method have been consistent with independent observations, the largest error is instead thought to arise from the EBSP orientation measurement (±5°).[5,15]

The data set included 479 grain-boundary groove traces collected from the circumferencial grooves around 10 island grains. The domain of surface normals was parametrized in terms of the spherical angles, θ and ϕ, which ranged between 0° and 90°. This domain was then discretized in 15 units of $\Delta(\cos\theta)$ and $\Delta\phi$, so that the octant of the orientation space was divided into 15^2 cells of equal area. Because of the cubic symmetry, every distinguishable surface normal is represented six times in this octant. The surface normals at the groove roots covered the range of distinguishable orientations so that each cell had between 5 and 60 observations. The procedure to reconstruct the surface energies from the observations was conducted as previously described.[5] The relaxation parameter, determined by the inverse of 10 times the number of equations any one capillarity vector is involved in, was 0.000278. The numerical procedure was assumed to have converged when adjustments to the field of capillarity vectors are 1% of those in the first step. This occurred after 41 iterations.

III. Results

The AFM image in Fig. 1(a) shows a typical circumferential thermal groove formed by a 6-min anneal at 1400°C in air. The straight segments apparent on this boundary were found on many of the circumferential grooves. However, when indexed in the crystal reference frame, they did not correspond to a consistent low-index surface. Higher resolution images (see Fig. 1(b)) are used to extract the profiles (see Fig. 1(c)) from which the geometry is measured.[4] Although groove widths have a range of sizes, they all increase in width as they are annealed and measurements of the width as a function of time are all consistent with the $t^{1/4}$ behavior that is expected when grooves form by surface diffusion. Using these measurements, the surface diffusion coefficient of $SrTiO_3$ at 1400°C can be estimated to be in the range between 1×10^{-10} and 1×10^{-9} m^2/s, depending on the boundary. Considering the fact that anisotropy leads to a wide range of observed groove widths and the current results are not comprehensive, these observations appear to be consistent with the earlier result reported by Jin *et al.*[16] ($\sim 0.5 \times 10^{-10}$ m^2/s), which was derived from a single boundary.

The relative surface energy as a function of surface normal is illustrated in Fig. 2(a). Here, $\gamma(\mathbf{n})$ is plotted on a stereographic projection along (100), with relative energy indicated by the shading. A plot of the energy around the perimeter of the standard stereographic triangle is shown in Fig. 3. The minimum energy is at (100), and the total anisotropy is 10%. To make an assessment of the uncertainty in the energy model, we quantify the extent to which it satisfies the equilibrium equations. Each discrete surface normal is involved in as many as 360 equilibrium equations. While the right-hand side of Eq. (1) is ideally zero, in practice there will be a small residual. Assuming that the source of the residual is evenly distributed among the three interfaces at the junction, we assign one-third of the residual to the surface normal of interest. We can then adjust the energy of the orientation by this amount to create a hypothetical corrected energy. Since this process can be repeated for each equation a surface normal is involved in, we can define a distribution of corrected energies with a standard deviation that is determined by the variation in the magnitudes of the residuals. Thus, the standard deviation of these corrected energies is a measure of how well the energy model actually satisfies all the equations; we use this quantity as a measure of the uncertainty. These standard deviations are plotted in Fig. 2(b) and illustrate that the typical uncertainty, with respect to satisfying the condition for local equilibrium, is about 0.03. This plot also shows that the error is sharply peaked at the (110) orientation. On the basis of this analysis, we assign the following values for the relative energies and uncertainties (the units are arbitrary):

$$\gamma_{100} = 0.93 \pm 0.03$$

$$\gamma_{110} = 1.01 \pm 0.06$$

$$\gamma_{111} = 1.02 \pm 0.01$$

The result from the capillarity vector reconstruction method is a discrete set of data. To communicate the data, a continuous function is more convenient. Therefore, a series fit to the result is given in the Appendix.

In addition to $\gamma(\mathbf{n})$, the method also produces a value for the relative grain-boundary energy. The energies of the 10 boundaries are listed in Table I. These data display the general trend that, in the low-misorientation-angle range, the grain-boundary energy increases with misorientation angle. There are departures from this trend, but this is to be expected since grain boundaries with different misorientation axes are expected to have different energies. Furthermore, the boundary energy also depends on the interface plane, and this effect is neglected in the present analysis.

AFM observations on the surfaces of different grains showed that some surfaces were flat and others were faceted. The flat surfaces are assumed to be part of the equilibrium crystal shape, while the faceted surfaces are assumed to be missing orientations. Of the faceted orientations, surfaces composed of two facets (see Fig. 4(a)) and three facets (see Fig. 4(b)) were found. An image of a surface with no detectable facets has already been presented in Fig. 1(b). The plot of surface structure as a function of crystallographic orientation on a standard stereographic triangle (see Fig. 5) is referred to as an orientation stability plot. Note that the open diamond near the center of the standard stereographic triangle corresponds to the surface illustrated in Fig. 4(b) and the one near (111) corresponds to the surface illustrated in Fig. 4(a). The plot reveals the trends that flat orientations occur in distinct fields surrounding the (100) and (110) poles and that other orientations

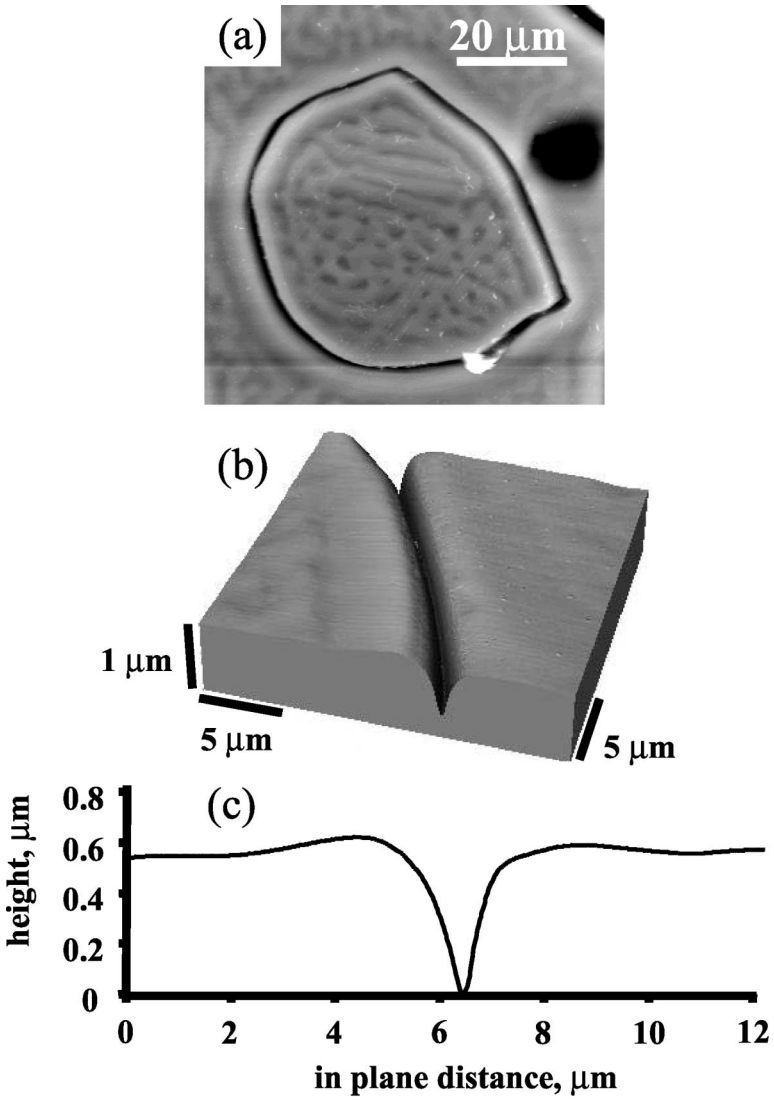

Fig. 1. (a) Topographic AFM image showing one of the included grains. The black-to-white contrast is ~500 nm. (b) Three-dimensional rendering of a higher resolution image of a section of a groove. (c) Sample groove profile, taken perpendicular to the triple line, used for measurements of the groove geometry.

are faceted. While no perfectly flat surfaces were found near the (111) orientation, these faceted surfaces were made up of large, flat (111) terraces, separated by steps with heights greater than 2 nm (see Fig. 4(a)). This suggests that the (111) surface is part of the equilibrium crystal shape but that, for surfaces near this orientation, the steps bunch to form facets with inclined orientations. This is in contrast to orientations close to the (110) and (100) surfaces, where single-layer steps tend to be separated so that the surface remains flat and a wider range of stable orientations are permitted. The current findings are consistent with observations reported at lower temperatures.[17–19]

IV. Discussion

For the interpretation of the orientation stability data, two potential sources of uncertainty are worth special attention. The first is that orientation measurements by EBSP are expected to have an uncertainty of about 5°. Thus, the fields on the orientation stability plot for the flat and faceted regions are not expected to be perfectly separated. The second potential source of uncertainty arises from the assumption that the normal to each grain surface in the sample reference frame is parallel to the global sample normal. It is possible for the surface of an individual grain to tilt away from the plane of the sample surface. For example, the surface of one of the grains whose orientation is vicinal to (100) could tilt to a singular (100) orientation if all the steps move to the grain edge. If this had happened during our experiment, the range of stable surfaces around (100) and (110) would be exaggerated. While we have observed evidence for this process in samples with small grain sizes that were annealed for extended periods so that the facets coarsened, there is no indication that this affects the current measurements. Large-scale AFM images reveal no surface tilting, and the images in Fig. 4 show that facet coarsening is limited; facet periods remain less than 1 μm after the relatively short (6 min) anneal. For a single facet to extend across an entire grain in this sample, the facet period would have to reach an appreciable fraction of the average grain size, which is 90 μm.

Taken together, the results show that the (100) surface has an energy that is much lower than other orientations. If we define θ_{100} as the angle between ⟨100⟩ and **n**, then we can say that the relative energy increases as θ_{100} increases from 0° to 30°. Beyond 30°, all the surfaces have a relative energy that is ~10% greater than that of the (100) surface. While $\gamma(\mathbf{n})$ shows fluctuations of ±0.015 in this higher energy region, these variations are not significant when compared with the experimental uncertainty. The appearance of stable surfaces in the

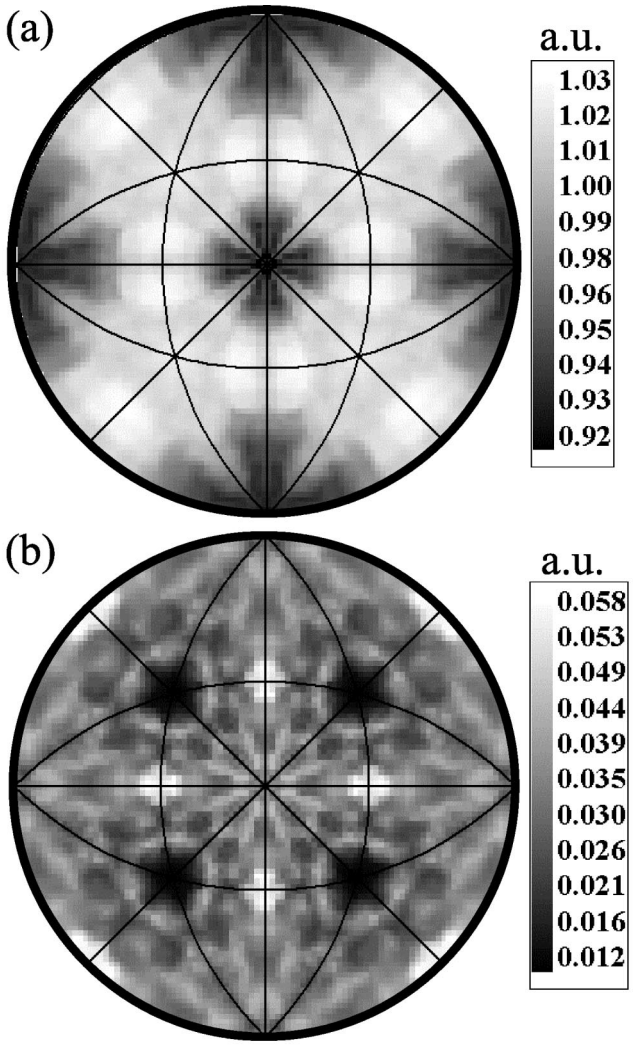

Fig. 2. (a) Density map on a (100)-oriented stereographic projection of the relative surface energies derived from the capillarity vector reconstruction method for $SrTiO_3$ at 1400°C. (b) Map of uncertainties determined by examining how well the energies satisfy the equilibrium condition. The scales are in arbitrary units.

vicinity of the (110) pole suggests that this orientation might have a significantly lower energy than indicated by the reconstructed $\gamma(\mathbf{n})$. Unfortunately, the uncertainty is maximized at this particular orientation.

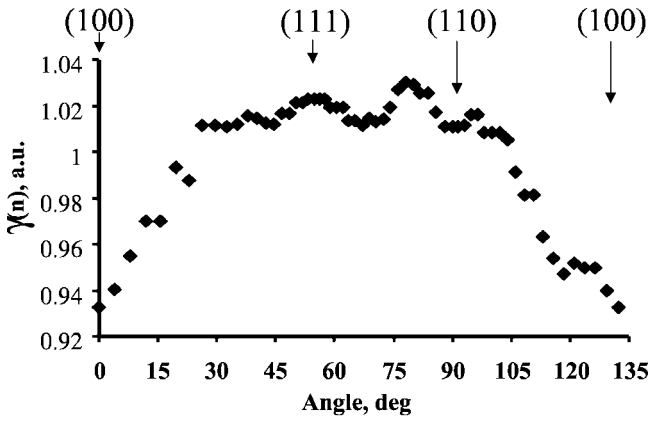

Fig. 3. Plot of relative surface energies around the perimeter of the unit triangle, from (100) to (111), then to (110), and back to (100).

Table I. Reconstructed Energies of Circumferential Boundaries

Misorientation angle (deg)	Energy (arbitrary units)
0.6	0.56
0.7	0.61
0.7	0.61
1.0	0.80
3.0	0.81
3.1	1.21
3.3	1.18
5.8	0.87
20.4	0.85
25.0	1.32

By applying the Wulff construction to $\gamma(\mathbf{n})$, we can determine an equilibrium crystal shape (ECS) and see if the missing orientations correlate with the orientation stability plot. In this discussion, we use the discrete reconstructed $\gamma(\mathbf{n})$. When we do this, we find that orientations within 15° of (100) and orientations within 5° of (110) are on the ECS; most of the other orientations are missing. While the consistency of this result with the orientation stability plot in Fig. 5 is satisfying, the ECS also contains features that are inconsistent with Fig. 5. For example, the Wulff construction leads to the result that several orientations inclined by about 15° from (111) are part of the ECS, while (111) is not. The appearance of these facets on the ECS is the result of a small downward fluctuation in the reconstructed $\gamma(\mathbf{n})$ at these surface normals (note in Fig. 3 that $\gamma(\mathbf{n})$ decreases by a small amount for surfaces inclined from (111)). Since this downward fluctuation is within the experimental uncertainty, it should not be considered significant. This illustrates two important points. The first is that small changes in $\gamma(\mathbf{n})$, within the range of the experimental uncertainty, can have dramatic effects on the ECS. The second is that the current experimental techniques do not have the precision to exactly determine the ECS from observations of thermal grooves.

On the other hand, by combining the reconstructed $\gamma(\mathbf{n})$ with the orientation stability data from observations of surface faceting, it is possible to develop an acceptable model for the ECS. For example, from $\gamma(\mathbf{n})$ and the orientation stability map, we know that (100) and (110) surfaces are on the ECS, as are surfaces close to these orientations. Furthermore, the appearance of (111) terraces on faceted surfaces in the vicinity of this orientation indicates that it too is part of the ECS. Surfaces not on the ECS are bound by either two or three facets. While current measurements do not exactly define the boundaries between the two- and three-facet regions, the surfaces with three-facets are clustered near the center of the standard stereographic triangle; an example of such a surface is illustrated in Fig. 4(b). The three-facet planes are {111}, a complex plane about 5° from {110}, and a complex plane inclined by about 15° from {100}. Orientations on great circles connecting two surfaces that are part of the ECS break up into two facets. For example, within experimental error, the surface in Fig. 4(a) is on the great circle joining (111) and a complex plane near (100). Similar surfaces are observed along the other lines that connect orientations that are part of the ECS.

Based on this information, the ECS should be approximately cube-shaped, with the edges and corners truncated by {110} and {111} planes. Furthermore, while the {111} facets will be very flat, the presence of surfaces vicinal to {100} and {110} means that the flat, low-index facets will be surrounded by curved surfaces meeting each other at sharp edges. The ECS illustrated in Fig. 6 reflects the above considerations and is consistent with both the reconstructed energy and the orientation stability data. While the identities of the surfaces that are part of the ECS and the places that they intersect are relatively certain, other features that depend on the details of the function are less certain. For example, the shape features six equivalent caps made up of {100} and surfaces inclined by $\leq$15°. While the size of the cap is relatively certain, the relative areas of each of the surfaces that make up the cap are

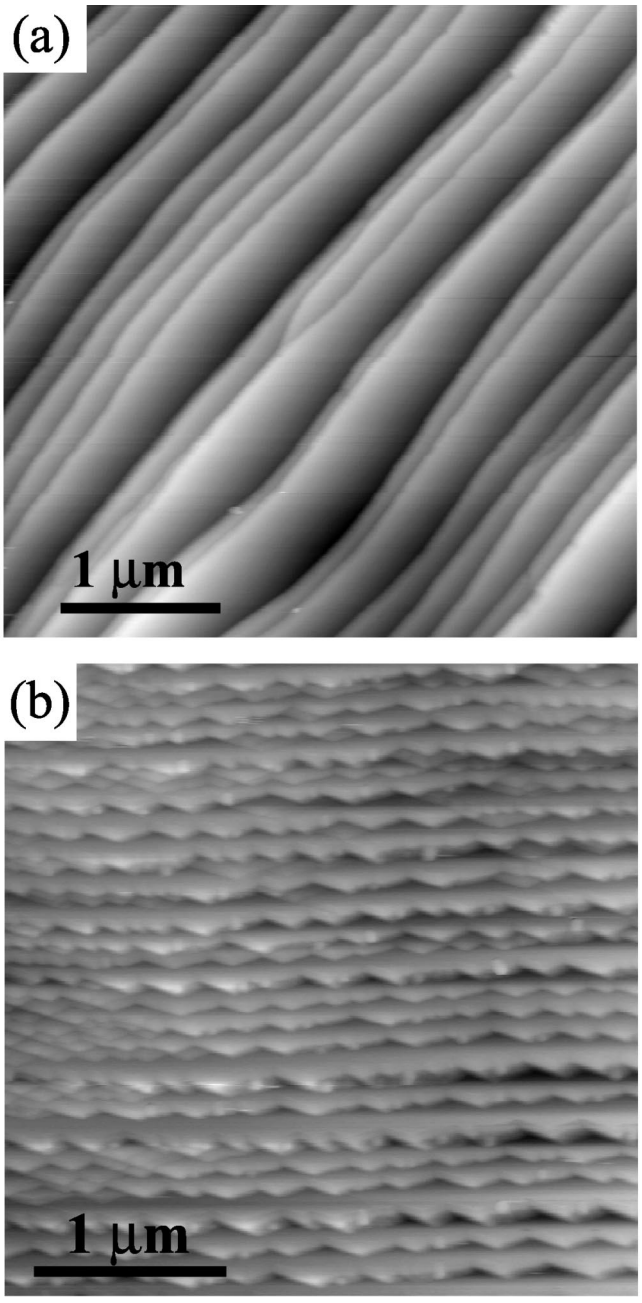

Fig. 4. AFM topographic images illustrating characteristic facet patterns observed on $SrTiO_3$ surface heated at 1400°C: (a) a surface bound by two facets and (b) a surface bound by three facets.

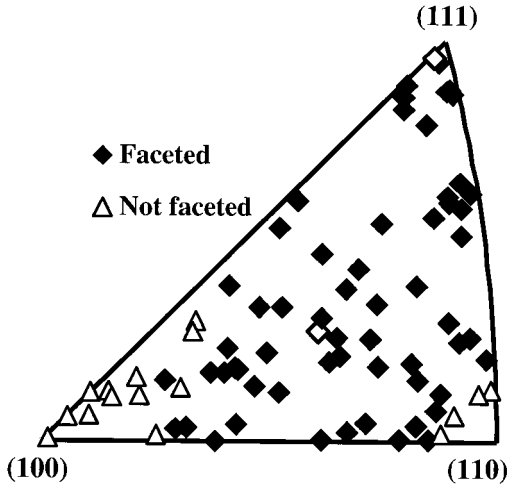

Fig. 5. Orientation stability map for $SrTiO_3$ at 1400°C. Each point corresponds to the orientation of an observed grain. Grains that were faceted are marked with a diamond, and grains that were smooth are marked with a triangle. The open diamonds correspond to the surfaces in Fig. 4; the one near (111) is shown in Fig. 4(a), and the one closer to the center is shown in Fig. 4(b).

uncertain. The cap might be gently curved, with each surface making up a roughly equal contribution to the total area, or it might be a mostly flat {100} surface with the curvature concentrated near the edges where it meets {111} and a surface near {110}.

The relative stability of orientations vicinal to (100) can have important consequences for the surface engineering of substrates for heteroepitaxial films. Processes designed to produce flat, well-ordered surfaces often involve elevated temperature annealing.[17] The current results indicate that slightly misaligned (100) substrates are thermally stable against the development of large facets so that when processed at high temperature, the steps will remain separated and the surfaces flat. Substrates misaligned from the (111) orientation, on the other hand, will be susceptible to faceting.

The low measured energy of the (100) surface is not surprising when one considers simple bulk termination models. While it is difficult to predict the relaxation processes involved in surface formation, the first-order contribution to the surface energy from the bond rupture process is relatively easy to estimate. When the perovskite structure is cleaved parallel to (100), one Ti–O and four Sr–O bonds are ruptured. To create the (110) surface, at least two Ti–O and five Sr–O bonds must be ruptured. To create the (111) surface, at least three Ti–O and three Sr–O bonds must be ruptured. If we take Pauling's[20] electrostatic bond valences (s) to be measures of the relative bond energies, then the Ti–O bond has a strength of 2/3 and the Sr–O bond a strength of 1/6. Therefore, the ratios of the total bond valences lost during the creation of each surface are $s_{110}/s_{100} = 1.62$ and $s_{111}/s_{100} = 1.87$. So, creating (110) and (111) surfaces requires the rupture of a larger number of stronger bonds than creating the (100) surface. This conclusion is consistent with the observation that (110) and (111) have similar energies that are significantly higher than (100).

Electrostatic considerations also suggest that the (100) surface energy should be lower than the others. When this surface is created by cleavage, equal areas of TiO_2-terminated crystal and SrO-terminated crystal must be created. Each of these surfaces is charge neutral and referred to as nonpolar. In other orientations, however, cleavage leaves charged surface termination layers that are usually referred to as polar surfaces. For example, when the

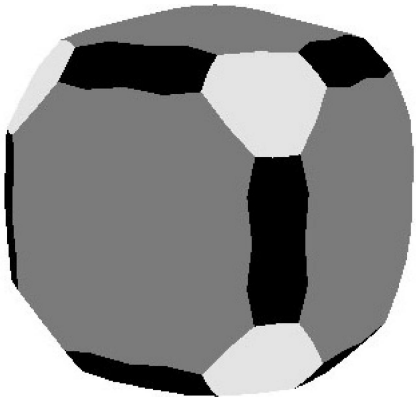

Fig. 6. Schematic equilibrium crystal shape constructed on the basis of the information in Fig. 3 and Fig. 5. The lightest shade is {111}, the intermediate shade is {100} and surfaces inclined from this orientation by ≤15°, and the darkest shade is {110} and surfaces inclined from this orientation by ≤5°.

Table II. Summary of Calculated Surface Energies

Surface energy (J/m^2)					
(100)		(110)		(111)	
SrO	TiO_2	SrTiO	O_2	SrO_3–Ti	Method
1.10	0.89				Electrostatic model[22]
1.33					Self-consistent pseudopotential[23,24]
		1.9		2.4	Semiempirical Hartree–Fock[25]
1.27					Self-consistent pseudopotential[26]
1.40	1.45	3.1†	2.2‡		Electrostatic shell model[27]
1.23§	1.28§				Density functional theory[28]
1.39§	1.43§				Ab initio Hartree–Fock[28]
1.80					Density functional theory/LDA[29]

†Average of quantities reported separately for Sr and TiO terminated surfaces.
‡Average of quantities reported separately for two different terminated surfaces.
§Represents an average of several similar calculations.

(110) surface is formed, equal areas of complementary $SrTiO^{4+}$ and O_2^{4-} surfaces are created. When the (111) surface is formed, equal areas of complementary SrO_3^{4-} and Ti^{4+} surfaces are created. Recent studies of the surfaces of single crystals suggest that both polar terminations coexist on surfaces annealed in air at 1200°C.[19] Because polar surfaces have permanent dipole moments, they are expected to have relatively higher energies.[21] Therefore, as we tilt away from the nonpolar (100) orientations, we expect the dipolar charge on the surface to increase and this can contribute to the increase in the energy.

The experimental measurement of the surface energy and the considerations above are all consistent with theoretical calculations of the surface energy of $SrTiO_3$.[22–29] These results are summarized in Table II. Strict comparisons between the results are difficult, since different physical models served as a basis for the calculations and, in the case of the (110) surface, different models for the surface termination layer were assumed. Taken in aggregate, however, the calculations are consistent with the observation that the (100) surface has the lowest energy and that the (110) and (111) surface energies are higher.

The circumferential groove method of determining the surface energy anisotropy and equilibrium crystal shape has both advantages and disadvantages when compared with the direct observation of pore shapes.[1–3,30] The obvious disadvantage is that it is an indirect measurement and the result is subject to the way in which the data are analyzed. Random errors in the orientation measurements and neglecting the influence of the variations in the grain-boundary energy as a function of interface plane lead to uncertainties in $\gamma(\mathbf{n})$ that leave details of the ECS in question. On the other hand, the direct observation of pores leaves little doubt about the ECS. While this method is superior in its ability to place the relative energies of singlular facets, it is more difficult to specify the nonsingular portions of the ECS (if they exist). Among the advantages of the circumferential groove method is that kinetically limiting nucleation barriers, that might limit observable pore shapes, do not influence thermal groove shape.[31,32] Another advantage is that the method is widely applicable to any polycrystalline microstructure which includes a small fraction of island grains.

V. Conclusions

The capillarity vector reconstruction method has been used to develop a model for the anisotropy of the surface energy of $SrTiO_3$ at 1400°C. The results indicate that the (100) surface has the lowest energy, that the energy increases with the inclination angle for surfaces inclined between 0° and 30° from (100), and that orientations inclined by more than 30° from (100) have similar energies that are about 10% higher. These results are consistent with the study of surface facets, which also indicate that the (111) surface, surfaces within 15° of (100), and surfaces within 5° of (110) are all part of the equilibrium crystal shape.

Table III. Fourier Coefficient for Function Fitted to $\gamma(n)$

a_{10}	0.581	b_{10}	0.550				
a_{11}	−0.061	b_{11}	−0.146	c_{11}	−1.100	d_{11}	−0.899
a_{20}	−0.106	b_{20}	−0.129				
a_{21}	0.206	b_{21}	0.294	c_{21}	−0.242	d_{21}	−0.333
a_{22}	−0.191	b_{22}	−0.353	c_{22}	0.116	d_{22}	0.270

Appendix

To represent the surface energy of $SrTiO_3$ at 1400°C as a continuous function, a two-dimensional Fourier series is fit to the discrete data. The surface normal vector, **n**, was parametrized by the spherical angles θ and ϕ. This allows the series to be written in the following way:

$$\gamma(\theta, \phi) = \gamma_{100} + \sum_{i=1}^{R}\sum_{j=0}^{R}[a_{ij}\{\cos(2i\theta) - 1\}\cos(j\phi) + b_{ij}\sin(2i\theta)\cos(j\phi) + c_{ij}\{\cos(2i\theta) - 1\}\sin(j\phi) + d_{ij}\sin(2i\theta)\sin(j\phi)\}] \quad \text{(A-1)}$$

We found that a series with $R = 2$ provided an adequate representation of the data (within experimental uncertainties), and the best fit coefficients are given in Table III. Throughout most of the range, the series provides a good approximation to the discrete results. However, small cusps which appear at (110) and (111) are artifacts of the basis functions used to construct the finite series and not a characteristic of the measured energy distribution.

References

[1]J.-H. Choi, D.-Y. Kim, B. J. Hockey, S. M. Wiederhorn, C. A. Handwerker, J. E. Blendell, W. C. Carter, and A. R. Roosen, "Equilibrium Shape of Internal Cavities in Sapphire," *J. Am. Ceram. Soc.*, **80** [1] 62–68 (1997).

[2]M. Kitayama and A. M. Glaeser, "The Wulff Shape of Alumina: III, Undoped Alumina," *J. Am. Ceram. Soc.*, **85** [3] 611–22 (2002).

[3]J.-H. Choi, D.-Y. Kim, B. J. Hockey, S. M. Wiederhorn, J. E. Blendell, and C. A. Handwerker, "Equilibrium Shape of Internal Cavities in Ruby and the Effect of Surface Energy Anisotropy on the Equilibrium Shape," *J. Am. Ceram. Soc.*, **85** [7] 1841–44 (2002).

[4]D. M. Saylor, D. E. Mason, and G. S. Rohrer, "Experimental Method for Determining Surface Energy Anisotropy and Its Application to Magnesia," *J. Am. Ceram. Soc.*, **83** [5] 1226–32 (2000).

[5]D. M. Saylor and G. S. Rohrer, "Evaluating Anisotropic Surface Energies Using the Capillarity Vector Reconstruction Method," *Interface Sci.*, **9** [1/2] 35–42 (2001).

[6]C. Herring, "Surface Tension as a Motivation for Sintering"; pp. 143–79 in *The Physics of Powder Metallurgy*. Edited by W. E. Kingston. McGraw-Hill, New York, 1951.

[7]D. W. Hoffman and J. W. Cahn, "Vector Thermodynamics for Anisotropic Surfaces. I. Fundamentals and Application to Plane Surface Junctions," *Surf. Sci.*, **31** [1] 368–88 (1972).

[8]J. W. Cahn and D. W. Hoffman, "Vector Thermodynamics for Anisotropic Surfaces. II. Curved and Faceted Surfaces," *Acta Metall.*, **22** [10] 1205–14 (1974).

[9]A. Morawiec, "Method To Calculate the Grain Boundary Energy Distribution over the Space of Macroscopic Boundary Parameters from the Geometry of Triple Junctions," *Acta Mater.*, **48** [13] 3525–32 (2000).

[10]M. Kawasaki, K. Takahashi, T. Maeda, R. Tsuchiya, M. Shinohara, O. Ishiyama, T. Yonezawa, M. Yoshimoto, and H. Koinuma, "Atomic Control of the $SrTiO_3$ Crystal Surface," *Science (Washington, DC)*, **266** [5190] 1540–42 (1994).

[11]R. A. McKee, F. J. Walker, and M. F. Chisholm, "Crystalline Oxides on Silicon: The First Five Monolayers," *Phys. Rev. Lett.*, **81** [14] 3014–17 (1998).

[12]The naming of commercial equipment does not imply endorsement by the National Institute of Standards and Technology.

[13]W. W. Mullins, "Theory of Thermal Grooving," *J. Appl. Phys.*, **28** [3] 333–39 (1957).

[14]C. A. Handwerker, J. M. Dynys, R. M. Cannon, and R. L. Coble, "Metal Reference Line Technique for Obtaining Dihedral Angles from Surface Thermal Grooves," *J. Am. Ceram. Soc.*, **73** [5] 1365–70 (1990).

[15]D. M. Saylor and G. S. Rohrer, "Measuring the Influence of Grain-Boundary Misorientation on Thermal Groove Geometry in Ceramic Polycrystals," *J. Am. Ceram. Soc.*, **82** [6] 1529–36 (1999).

[16]M. Jin, E. Shimada, and Y. Ikuma, "Grain Boundary Grooving by Surface Diffusion in $SrTiO_3$ Bicrystal," *J. Mater. Res.*, **14** [6] 2548–53 (1999).

[17]T.-D. Doan, J. L. Giocondi, G. S. Rohrer, and P. A. Salvador, "Surface Engineering along the Close-Packed Direction of Perovskite Oxides," *J. Cryst. Growth*, **225** [W2–4] 178–82 (2001).

[18]J. L. Giocondi and G. S. Rohrer, "Orientation Dependence of Photochemical Reduction Reactions on $SrTiO_3$ Surfaces," *Mater. Res. Soc. Symp. Proc.*, in press.

[19]J. L. Giocondi and G. S. Rohrer, "Structure Sensitivity of Photochemical Oxidation and Reduction Reactions on $SrTiO_3$ Surfaces," *J. Am. Ceram. Soc.*, **86** [7] 1182–89 (2003).

[20]L. Pauling. "The Principles Determining the Structure of Complex Ionic Crystals," *J. Am. Chem. Soc.*, **51**, 1010–26 (1929).

[21]P. W. Tasker, "The Stability of Ionic Crystal Surfaces," *J. Phys. C: Solid State Phys.*, **12** [22] 4977–84 (1979).

[22]W. C. Mackrodt, "Atomistic Simulation of Oxide Surfaces," *Phys. Chem. Miner.*, **15** [3] 228–37 (1988).

[23]J. Padilla and D. Vanderbilt, "Ab Initio Study of $SrTiO_3$ Surfaces," *Surf. Sci.*, **418** [1] 64–70 (1998).

[24]B. Meyer, J. Padilla, and D. Vanderbilt, "Theory of $PbTiO_3$, $BaTiO_3$, and $SrTiO_3$ Surfaces," *Faraday Discuss.*, **114**, 395–405 (1999).

[25]A. Pojani, F. Finocchi, and C. Noguera, "Polarity on the $SrTiO_3$ (111) and (110) Surfaces," *Surf. Sci.*, **442** [2] 179–98 (1999).

[26]C. Cheng, K. Kunc, and M. H. Lee, "Structural Relaxation and Longitudinal Dipole Moment of $SrTiO_3$ (001) (1×1) Surfaces," *Phys. Rev. B*, **62** [15] 10409–18 (2000).

[27]E. Heifets, E. A. Kotomin, and J. Maier, "Semiempirical Simulations of Surface Relaxation for Perovskite Titanates," *Surf. Sci.*, **462** [1–3] 19–35 (2000).

[28]E. Heifets, R. I. Eglitis, E. A. Kotomin, J. Maier, and G. Borstel, "*Ab Initio* Modeling of Surface Structure for $SrTiO_3$ Perovskite Crystals," *Phys. Rev. B*, **64** [23] 235417–22 (2001).

[29]X. Zhang and A. Demkov, "Steps on the (001) $SrTiO_3$ Surface," *J. Vac. Sci. Technol., B*, **20** [4] 1664–70 (2002).

[30]T. Narushima and A. M. Glaeser, "High-Temperature Morphological Evolution of Lithographically Introduced Cavities in Silicon Carbide," *J. Am. Ceram. Soc.*, **84** [5] 921–28 (2001).

[31]W. W. Mullins and G. S. Rohrer, "Nucleation Barrier for Volume Conserving Shape Changes of Faceted Crystals," *J. Am. Ceram. Soc.*, **83** [1] 214–16 (2000).

[32]G. S. Rohrer, C. L. Rohrer, and W. W. Mullins, "Nucleation Energy Barriers for Volume Conserving Shape Changes of Crystals with Nonequilibrium Morphologies," *J. Am. Ceram. Soc.*, **84** [9] 2099–104 (2001). □